J Ther Eng, Vol. 9, No. 5, pp. 1189−1207, September, 2023

Journal of Thermal Engineering
Web page info: https://jten.yildiz.edu.tr
DOI: 10.18186/thermal.1372168

Journal of Thermal Engineering

Research Article

Extended experimental investigation of a double-effect active solar still with a paraffin wax, in Owerri, Nigeria

Ernest C. NWOSU[1,*], Kelechi NSOFOR[1], Godswill N. NWAJI[1], Chibuike ONONOGBO[1], Ikechi OFONG[1], Nnamdi V. OGUEKE[1,2], Emmanuel E. ANYANWU[1]

[1]*Department of Mechanical Engineering, Federal University of Technology Owerri, P.M.B., Imo State, 1526, Nigeria*
[2]*African Center of Excellence in Future Energies and Electrochemical Systems (ACE-FUELS), Federal University of Technology Owerri, P.M.B. 1526, Imo State, 1526, Nigeria*

ARTICLE INFO

Article history
Received: 11 May 2022
Revised: 10 November 2022
Accepted: 09 December 2022

Keywords:
Solar Distillation; Double Effect; Thermal Performance; Productivity; PCM

ABSTRACT

In this work, an experiment-based study of a double-effect, single-slope active solar still (SSASS) is presented. The system comprises an upper and a lower basin incorporated with a paraffin wax acting as a phase change material (PCM). The use of phase change materials is very important due to their high storage density and the isothermal nature of the storage process. Paraffin wax was selected based on its attractive thermo-physical properties. The thermal behaviours of the system during the diurnal and nocturnal phases in both compartments were explored. Experimental results showed that the upper basin's yield contributed more to the overall distillate production over a 24-hour cycle while that of the lower basin predominated the diurnal production. Though the PCM served as an energy source during the nocturnal phase, it did not translate to significant improvement in the yield of the lower basin. The heat retention ability of the lower glazing retarded the condensation of the humid air in the lower compartment during the off-sunshine period. Thus, the nocturnal yield of the system was largely driven by the improved temperature difference between the upper saline water and the upper glazing, as well as the stored thermal energy in the saline water mass before sunset. The system achieved a maximum yield of 2,450 ml/day and a yield rate of 232.5 ml/h. A maximum monthly average yield of 1,787 ml/day was realized in May and a minimum of 692 ml/day in July. Nocturnal distillate production accounted for an average of 55% of the total distillate recovered from the still daily. The system achieved an efficiency range of 12.20 - 32.21%. The cost of freshwater production from the system is estimated at 0.0508 $/L with a payback period of 267 days. Thus, this system is economically viable and suitable particularly, for low-income earners.

Cite this article as: Nwosu EC, Nsofor K, Nwaji GN, Ononogbo C, Ofong I, Ogueke NV, Emmanuel E. Anyanwu EE. Extended experimental investigation of a double-effect active solar still with a paraffin wax, in Owerri, Nigeria. J Ther Eng 2023;9(5):1189−1207.

***Corresponding author.**
*E-mail address: nwosuernest@gmail.com

This paper was recommended for publication in revised form by Editor Tolga Taner

INTRODUCTION

Clean and adequate drinking water deficiency poses a serious threat to the existence of many, especially those in developing countries. A study by the United Nations Children's Fund (UNICEF) reports that 26.5 million Nigerian children are currently facing water vulnerability. Unfortunately, it is also a global problem, with 450 million children currently lacking access to potable water [1]. At the current exponential rate of population growth, these figures are only going to rise in the coming years. Water scarcity occurs when there are insufficient water resources to meet the demand of a region. This phenomenon is largely driven by climate change and the rapid depletion of freshwater resources. Incidentally, man's activities are largely responsible for the current state of freshwater shortage. Overdependence on groundwater sources, due to increased demand, and the channelling of industrial waste into rivers make up some of the reasons for the clean water scarcity plaguing some areas of the world.

To ease the pressure on available freshwater resources, alternative means of providing clean water should be sought. Water desalination techniques such as reverse osmosis are largely effective but expensive and energy-intensive, in addition to the increased levels of greenhouse emissions associated therein [2]. Hence, the need to develop efficient and eco-friendly sustainable solutions for water desalination is paramount. Solar distillation of seawater offers such an alternative in a small-scale, decentralized, and environmentally friendly manner. Seawater is largely abundant and can therefore be harnessed while easing the pressure on groundwater resources. In turn, solar energy is free and can be effectively harnessed without any side effects on the environment.

Solar distillation is a process in which the energy of the sun is used to evaporate freshwater from saline or brackish water in a device commonly known as a solar still. Solar stills operate on the basic principles of evaporation and condensation and are categorized in terms of energy supply as passive and active distillation. In passive solar distillation, solar energy is the only source of thermal energy while active solar distillation involves the use of additional thermal energy for faster evaporation.

Conventional solar distillation involves passive solar stills with single-effect condensation. However, they are not widely deployed due to low thermal efficiency and poor distillate yield. To address these issues, single-effect solar stills with design features like concentrators, evacuated tube collectors, stepped absorbers, blackened steel balls, etc. have been tested to varying positive results. Kedar et al. [3] developed a model of a hybrid solar desalination unit consisting of an evacuated tube collector (ETC) and a compound parabolic concentrator (CPC). The unit achieved a distillate yield of 2 L/day for an absorber area of 1.6 m^2. Mouhsin et al. [4] conducted a study on a novel cascade solar still with a stepped absorber plate integrated with baffles. The system recorded a maximum hourly yield of 412 ml/m^2.hr and a performance improvement of 17.7% in comparison to a single-basin still. In the same vein, Diabil [5] enhanced the productivity of a single-basin still by increasing the evaporation surface area using blackened stainless-steel balls. For steel balls diameter of 10 mm, the system achieved a performance improvement of 38.07% compared to a conventional solar still.

Efforts have been made in the yield improvement of solar stills through the provision of an extra condensing surface. In this configuration, the latent heat of condensation from the first effect is utilized in heating water in the subsequent effect. Working with a double-basin still, Al-Karaghouli and Alnaser [6] recorded a yield improvement of 40% compared to a conventional still. Similarly, Agboola et al. [7] recorded a yield improvement of 48.1% with a double-basin still against a single-basin still. In a bid to improve the productivity of a double-effect solar still, Panchal [8] coupled vacuum tubes to the lower basin of the still and recorded an improvement of 56%. El-Sebaey [9] designed a double-effect solar still with a stepped upper basin made of a 3 mm thick acrylic sheet. The system recorded improvements of 59.9% and 61.3% in yield and thermal efficiency, respectively. To exploit the temperature difference and latent heat of condensation in the lower basin of a double-effect still, Zurigat and Abu-Arabi [10] developed a model of a regenerative system. Provision was made for the flow of saline water over the surface of the lower glass cover while contributing to the distillate yield of the upper basin. The regenerative system achieved an improvement of 20% over a conventional solar still.

The arrangement for the utilization of latent heat of condensation can be extended beyond double-effect systems. Madhlopa and Johnstone [11] developed a passive triple-effect solar still with a separate condenser and recorded a yield improvement of 62% over a conventional still. Elsharif and Mahkamov [12] studied the effect of pressure on the performance of an evacuated four-stage solar still using a fluid piston energy converter. The system recorded daily yields of 39.9 and 25.95 kg/m^2 at pressures of 0.03 bar and atmospheric, respectively.

In recent times, a major development in the field of solar distillation has been found in using phase change materials as a means of thermal energy storage. Working with a single-basin still, Sonker et al. [13] evaluated the performances of lauric acid, stearic acid, and paraffin wax PCMs. The system recorded yield improvements of 71.6, 78.2, and 92.6% with lauric acid, stearic acid, and paraffin wax, respectively. Similarly, El-Sebaii [14] recorded a yield improvement of 80.2% for a single-basin solar still using stearic acid as the PCM. In the same vein, Kabeel et al. [15] enhanced the performance of a single-basin still using hot air injection and paraffin wax. The system achieved a daily yield of 9.36 L/m^2 against 4.5 L/m^2 recorded by the conventional still, which translates to an improvement of 108%. However, Ramasamy and Sivaraman [16] reported slight yield improvement in a stepped-basin solar still with paraffin wax as the PCM. This

is attributed to the fact that some of the energy gained by the absorber plate were observed as phase change energy in the PCM, thus inhibiting the diurnal performance of the system. Attempts have been made in improving the freshwater yield of solar stills using nanoparticles/PCM combination (NPCM). The addition of nanoparticles to the PCM enhances the Nusselt number and consequently, improves the heat transfer coefficient [17]. In this regard, Sharshir et al. [18] reported an improvement of 65% in freshwater yield of a single-basin solar still using a combination of flake graphite nanoparticles and paraffin wax PCM.

In addition to design and operational factors, the productivity of solar-powered distillation units is also influenced by environmental parameters. Boubekri and Chaker [19] evaluated the effect of reflectors on the seasonal performance of an active solar still in Algeria. The increase in yield due to reflectors was much more in the winter (72.8%); whereas in the spring and summer, it was 40.33 and 7.54%, respectively. These differences could be attributed to the daylight hours occasioned by the variations in declination during these periods. Egarievwe [20] evaluated the performance of a concrete-basin solar still during the harmattan season in the guinea savannah. The system recorded a mean daily yield of 1.069 L/m^2 and an efficiency of 17.6% during this period. The efficiency of the system improved with rainfall due to the cooling effect on the glass cover and the subsequent increase in condensation rate. Similarly, Ogunseye and Oladepo [21] observed an improvement in the yield of a solar still with an increase in the relative humidity of the ambience. The harmattan season in Nigeria is characterized by low humidity with little or no rainfall. Thus, the performance of the solar still was negatively impacted during this period due to the prevailing environmental conditions. These conditions vary throughout the year, hence there is a need for the evaluation of the seasonal performance of solar stills. At present, there is a paucity of information on the detailed performance of double-effect solar stills under different climatic conditions over 24 hours.

This study considers the behaviour of a prefabricated double-effect single-slope solar still integrated with a paraffin wax under different climatic conditions (dry and rainy seasons). The contributions of both diurnal and nocturnal phases to the overall yield as well as the economic viability of the system were assessed. Paraffin wax was chosen as the phase change material due to its availability and high latent heat.

METHODOLOGY

The flow diagram of the research methodology is shown in Figure 1. Firstly, a detailed design was performed to determine the respective dimensions of the still components, after which the system was constructed and assembled. The seasonal performance of the double-effect still was investigated through an extended experimental study. Finally, the harvested data were analyzed, and conclusions were drawn.

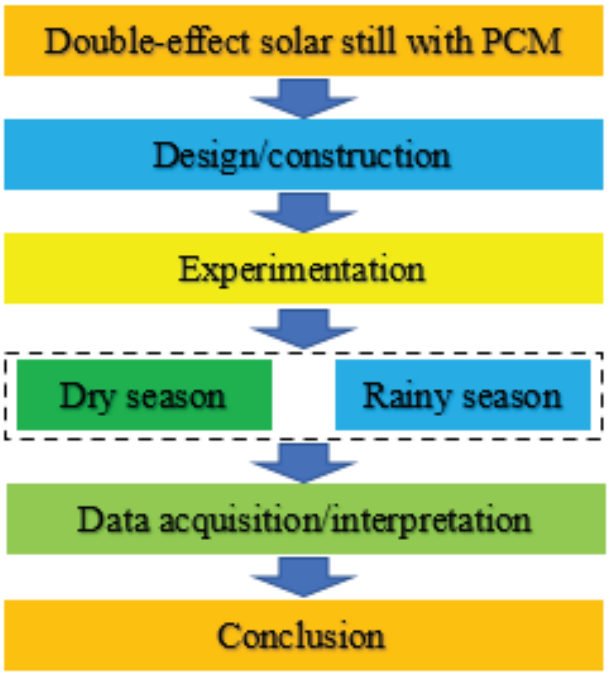

Figure 1. Flow diagram of the research methodology.

Experimental Design

The design of the double-effect solar still involves the analysis of the energy and mass transfers within and around the still structure as shown in Figure 2.

The assumptions and factors considered in deriving the energy-balanced equations for the design of the components of the solar still are stated below.

- The solar still is designed using average long-term data obtained from the month of minimum insolation of the test location.
- The area of the absorber plate and glazing are assumed to be equal due to the small pitch of the glazing.
- The basins are shallow and well insulated and as such the heat capacity terms are dropped and a steady-state condition is assumed.

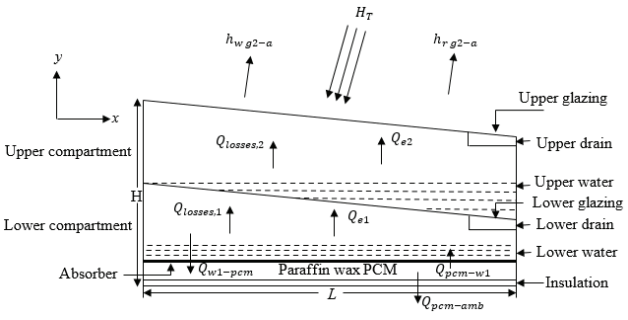

Figure 2. Schematic diagram of the double-effect single-slope solar still.

- The evaporative energy in both basins serves as the solar still output while the convective and radiative terms are grouped as losses.

From Figure 2, the daily evaporative energy from both basins is equal to the radiant energy absorbed by the lower and upper water, second glazing, and the energy output from the PCM minus the energy stored in the PCM and the external losses from the upper glazing. Thus, the overall energy balance in the system is expressed as

$$Q_{e1} + Q_{e2} = \left[H_T\tau_1\tau_2(\alpha_{ab} + \alpha_w)A_{ab} + H_T\tau_2(\alpha_g + \alpha_w)A_{g1} + H_T\alpha_g A_{g2} + Q_{pcm-ab}\right] - \left[Q_{ab-pcm} + \left[h_{r\,g2-a} + h_{w\,g2-a}\right](T_{g2} - T_a)A_{g2}\right] \quad (1)$$

where H_T is the mean daily irradiation incident on the solar still, A_{ab} is the area of the absorber, A_{g1} is the area of the lower (first) glazing, and A_{g2} is the area of the upper (second) glazing.

$h_{r\,g2-a}$ and $h_{w\,g2-a}$ are the radiative and wind convective loss coefficients from the top glazing to the ambient, respectively; while Q_{e1} and Q_{e2} are evaporative energy in the lower and upper basins, respectively.

Q_{ab-pcm} is the energy transferred from the absorber plate to the PCM during the charging phase. It is evaluated as given in Eq. (2) [13]:

$$Q_{ab-pcm} = \Delta t\left[\frac{k_{ab}}{X_{ab}}\right](T_{ab} - T_{pcm})A_{ab} \quad (2)$$

Q_{pcm-ab} is the energy transferred from the PCM to the absorber plate during the discharging phase. It is evaluated as given in Eq. (3) [13]:

$$Q_{pcm-ab} = \Delta t\left[\frac{k_{pcm}}{X_{pcm}}\right](T_{pcm} - T_{ab})A_{ab} \quad (3)$$

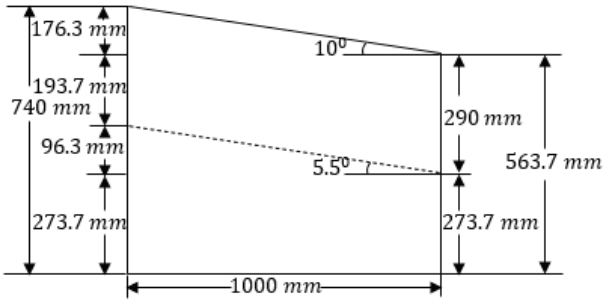

Figure 3. Design of the single-slope double-effect solar still.

The design of the single-slope double-effect solar still with the inclination angles and the side dimensions is shown in Figure 3.

Experimental Setup

Figure 4 shows a picture of the experimental setup of the single-slope double-effect solar still. The system was installed at the Department of Mechanical Engineering, Federal University of Technology Owerri (5.49°N, 7.02°E), Nigeria. The system was mounted facing south to harvest the maximum possible radiation during the experiments.

The system comprises a solar absorber under which is attached a mass of paraffin wax, a lower and an upper basin with glazing materials atop. A glass of 3.2mm thickness was chosen as the glazing material for the upper and lower basins. The absorber plate is made of galvanized steel and painted matte black to enhance its absorptivity. The specifications of the various system components and the properties of the PCM are listed in Tables 1 and 2, respectively.

From Figure 4, solar radiation is transmitted by the glazing system through the saline water bodies to the basin liner at the bottom of the still where it is absorbed. The

Figure 4. Picture of the experimental rig used for the study.

Table 1. Specifications of the double effect single slope solar still fabricated

Component	Specification
Top condensing cover	Transparent glass (low iron)
The base of the upper basin	Transparent glass (low iron)
The base of the lower basin	Black galvanized steel
Absorber area	1.10m^2
Absorber thickness	2mm
Breadth	1m
Length	1.1m
Glazing thickness	3.2mm
Top cover inclination	10^o
The combined front height of the upper and lower basins	0.5637m
The combined back height of the upper and lower basins	0.740m

Table 2. Thermo-physical properties of paraffin wax

Properties	Values
Specific heat capacity, C_p	2890 J/kg°C
Thermal conductivity, k	0.138 W/m°C
Melting point temperature, T^*	46.7 °C
Latent heat of fusion, λ	0.209 MJ/kg
Density, ρ	786 kg/m^3
Mass	7 kg

glazing materials block longwave radiation, thus acting as a heat trap to increase the absorber heat buildup. Some of the absorbed thermal energy is transferred to the lower saline water by convection, some to the PCM beneath the absorber plate by conduction, and the rest is lost to the ambient. The energy delivered to the lower saline water initiates evaporation at its interface. The air-vapour combination rises to the underside of the lower glazing where it loses its latent energy content due to condensation, thus leaving behind salts and bacteria in the saline water. The condensate drips down the lower glazing due to gravity and is collected in a measuring flask.

The upper saline water is heated using the latent heat generated during the condensation of vapour from the lower saline water as well as the transmitted radiant energy absorbed by it. This also causes evaporation of the upper saline water which after releasing its latent heat of vaporization, condenses on the underside of the upper glazing. The condensate subsequently flows into a measuring flask by gravity. By radiation to the sky and convection to the ambient air, the heat generated at the underside of the upper glazing during condensation is lost from the system. The energy stored in the PCM placed beneath the absorber plate is utilized during off-sunshine hours.

The experimental investigations were carried out between February to October 2020, covering the dry and rainy seasons in Nigeria. The investigation captured both the diurnal and nocturnal behaviours of the system. The test covered 12- and 24-hour cycles ranging from local time of 6:00 to 18:00 hours and 6:00 to 6:00 hours the next day. The upper and lower basins were cleaned at intervals to prevent the deposition of salts.

Instrumentation

Temperatures of the absorber, PCM, upper and lower saline water, upper and lower glazing, and the ambient were measured with the aid of K-type thermocouples and recorded on a 7-channel temperature data logger. The mean temperatures of these discrete points were recorded on a memory board programmed for a time interval of five minutes spanning a period of 12 and 24 hours. The recorded data were extracted from the data logger and transferred to a Microsoft Excel worksheet. The data logger was powered by a 12v/75Ah DC battery source. In situ solar radiation data at the solar still location was measured using a handheld digital solarimeter of a resolution, R of 0.1 W/m^2.

Table 3. Properties of measuring instruments

S/No	Instrument	Parameter	Accuracy	Range	% Error
1	Solar meter	Solar radiation	±1 <W/m^2	0.1-2000 W/m^2	±5%R
2	Thermocouple	Temperature	±0.2°C	-50 - 150°C	0.75%
3	Anemometer	Wind speed	±0.1 m/s	0 – 25 m/s	3%
4	Measuring cylinder	Distillate	±2 mL	0 – 1000 mL	2%

Wind speed was measured using a handheld digital anemometer, while the diurnal and nocturnal distillate yields were measured using a 1000 ml graduated measuring cylinder. The characteristics of the measuring devices are shown in Table 3.

Experimental Uncertainty Analysis

Experimental errors are encountered as a result of the measuring method, ambient conditions, and the inherent error of the measuring instrument. These errors are grouped as internal and external uncertainties. Internal uncertainty is associated with the experimental observations while external uncertainty is connected to the measuring instruments as depicted in Table 3. The percentage uncertainty of individual parameters for each set of observations is calculated with the following equations [22, 23]:

$$\sigma_i = \sqrt{\frac{\sum(X - \bar{X})^2}{N_0}} \quad (4)$$

$$U = \sqrt{\frac{\sum \sigma_i^2}{N^2}} \quad (5)$$

$$Percentage\ uncertainty = \frac{U}{Z} \times 100 \quad (6)$$

where σ_i is the standard deviation for each sample set, $N_o$is the number of observations in a sample set, $\bar{X}$ is the mean of a sample set, $(X - \bar{X})$ is the deviation of observations from the mean value, U is the experimental uncertainty, N is the total number of observations, and Z is the average of the total observations of a given parameter.

The hourly solar radiation values and that of the combined freshwater yield of a double-effect unit for selected days in April are shown in Table 4. The standard deviations and the percentage uncertainties of these parameters for the period under investigation were evaluated with the aid of Eqs. (4) – (6) and their values are presented in Table 4.

From Table 4, the percentage uncertainties of the solar radiation and freshwater yield for the period in April under consideration were found to be 3.16 and 1.53%, respectively. These values represent the degree of errors that crept in during the experimental observations, thus showing the level of confidence in the obtained results. Similarly, working with a basin-type solar still, Agrawal and Rana [22] and Prasad et al. [24] independently reported percentage uncertainties of 2.871 and 3.5% for solar radiation, and 3.187 and 1.5% for freshwater yield, respectively. In the same vein, Gaur et al. [25] recorded a total experimental uncertainty of 14.82 for a hybrid active solar still.

Table 4. Experimental uncertainties of a single-slope double-effect still in April

S/No	Time (h)	Solar radiation intensity (W/m²)					Freshwater yield (mL/m²/h)				
		10-Ap	25-Ap	26-Ap	28-Ap	30-Ap	10-Ap	25-Ap	26-Ap	28-Ap	30-Ap
1	6:00	0	0	0	0	0	0	0	0	0	0
2	7:00	27.9	57.8	71.3	45.6	46.8	17.1	16.7	16.9	35.7	20.6
3	8:00	314.3	285.4	205.2	291.5	211	36.6	35.7	36.2	76.6	44.2
4	9:00	798	299.9	480	594	512	50.2	48.9	49.6	104.9	60.7
5	10:00	309.3	431.9	890	873	349	58.7	57.3	57.9	122.8	70.9
6	11:00	462	619	1103	1076	836	62.5	61	61.8	130.8	75.6
7	12:00	1370	847.7	464	1113	641	61.7	60.2	60.9	129.1	74.6
8	13:00	1315	917.5	1313	1332	874	69.4	65.9	68.8	128.2	79.2
9	14:00	445	751	505	940	633.7	84.6	77.3	84.2	127.3	88.4
10	15:00	7	901.7	48	662	52.6	91.1	80.7	91	113.2	88.5
11	16:00	85.3	85	94	277	69.3	87.8	74.9	88.1	81.9	77.7
12	17:00	6.1	196	105.6	303.8	401.4	94.1	78.9	94.6	74.8	79.6
13	18:00	3.5	71.5	20.4	30	25.4	106.4	89.2	106.9	84.6	90
Daily Value (Total)		5143.4	5464.4	5299.8	7537.9	4652.2	819.9	746.9	816.9	1210	849.9
Mean ($\bar{X}$)		395.6	420.3	407.7	579.8	357.9	63.1	57.5	62.8	93.1	65.4
Standard deviation (σ)		465.9	332.3	424.6	437.9	305.1	30.02	25.3	30.2	38.5	26.6
Internal uncertainty (U)						13.69					1.048
Average of the total observations (Z)						432.3					68.37
% Uncertainty						3.167					1.53

RESULTS AND DISCUSSIONS

The double-effect solar still was tested in February, March, April, May, July, and October 2020, covering the major seasons (dry and rainy) in Nigeria.

DRY SEASON THERMAL PERFORMANCE OF THE STILL COMPONENTS

Nigeria's climate is broadly classified into two seasonal periods: dry and rainy seasons. The dry season encompasses November to March while the rainy season spans from April to October. However, within the dry season, there is the harmattan period which is associated with dry and dusty winds from the Sahara Desert across the country. The results obtained during the harmattan period are presented in Figures 5-7 while Figures 8 and 9 show the performance of the still components in March.

Figure 5 illustrates the behaviour of the wind speed and the solar radiation on 10th February 2020. The profiles of the solar radiation and the wind speed followed a similar trend with peak values of 899.1 W/m^2 at 14:00 hours and 3.1 m/s at 15:00 hours, respectively.

Figure 6 shows the diurnal temperature profiles of the still components on 10th February while Figure 7 shows three days (February 12 – 14, 2020) profiles of the solar still components during the harmattan period. From these

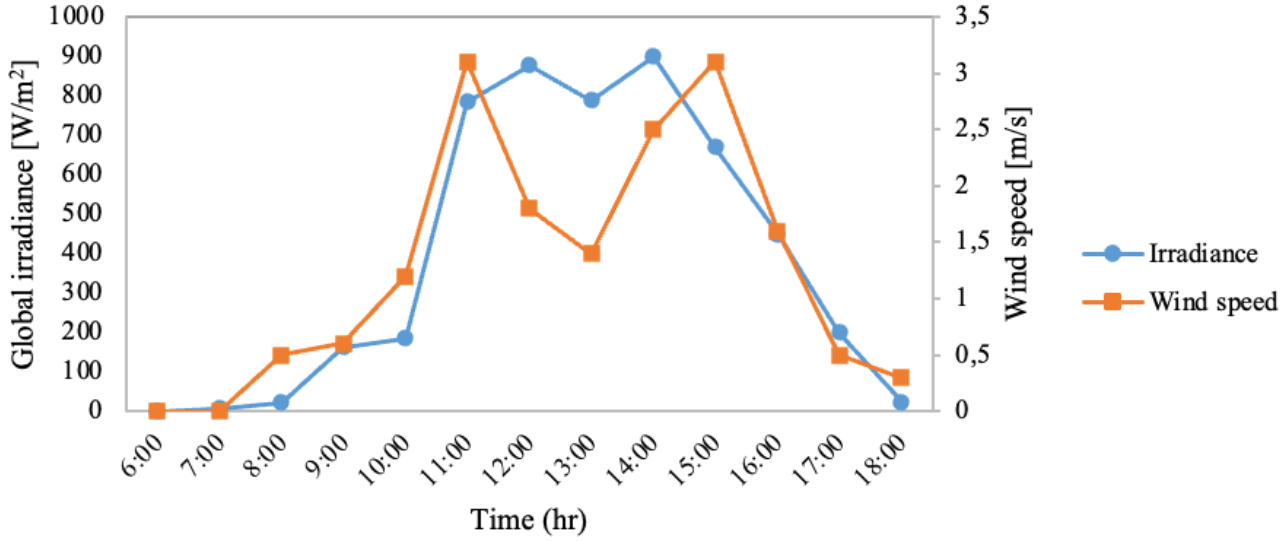

Figure 5. Variation of wind speed with solar radiation on 10th February 2020.

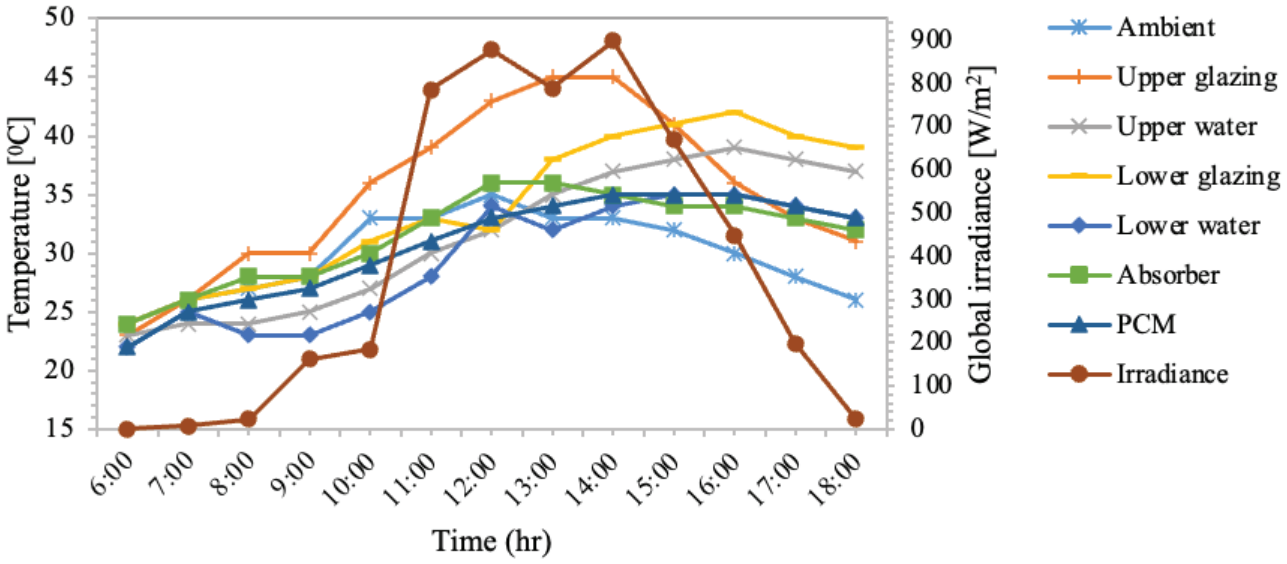

Figure 6. Temperature profiles of the still components with solar radiation on 10th February 2020.

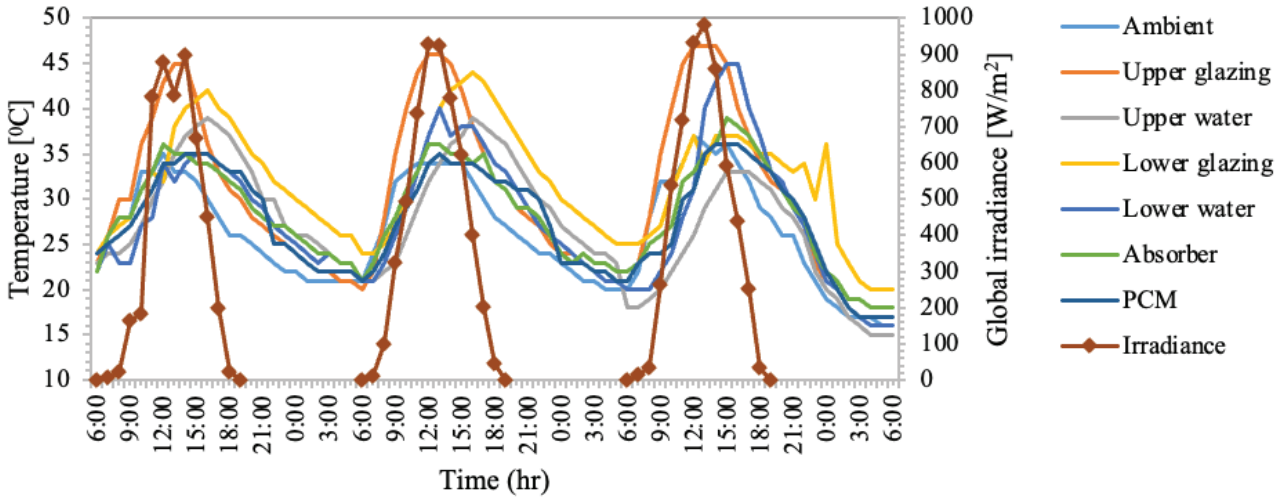

Figure 7. Three days temperature profiles of the still components with solar radiation in February 2020.

figures, as the solar radiation rises, there is a corresponding increase in the internal temperatures across the still components in response to the changes in ambient conditions. Unfortunately, lower-than-expected temperatures were recorded due to the very dusty atmosphere associated with the harmattan season. Within this period, surfaces are quickly covered by a heavy dusty layer which greatly affected the overall thermal performance of the solar still. The upper glazing is the most exposed component of the still, thus it is most likely to respond to little variations in ambient conditions. Thus, the upper glazing maintained high-temperature values till 15:00 hours as depicted in Figures6 and 7. The temperature build-up of the absorber and lower saline water did not improve much, thus impacting negatively on the performance of the system. This can be attributed to the effect of the harmattan haze which limited visibility and radiation during this period. A similar result was reported by Egarievwe et al. [20] during the harmattan season in Nigeria. The increase in the clearness index in March improved the beam component of solar radiation. Thus, the solar still components experienced an increase in temperature as depicted in Figures 8 and 9.

Figures 8 and 9 show the twenty-four-hour and diurnal temperature profiles of the solar still components on the 3rd and 13th of March, respectively. Figure 8 depicts a typical dry day that experienced an early evening shower after a very sunny morning and afternoon. The slight shower that occurred around 16:00 hours on this day led to a sharp drop

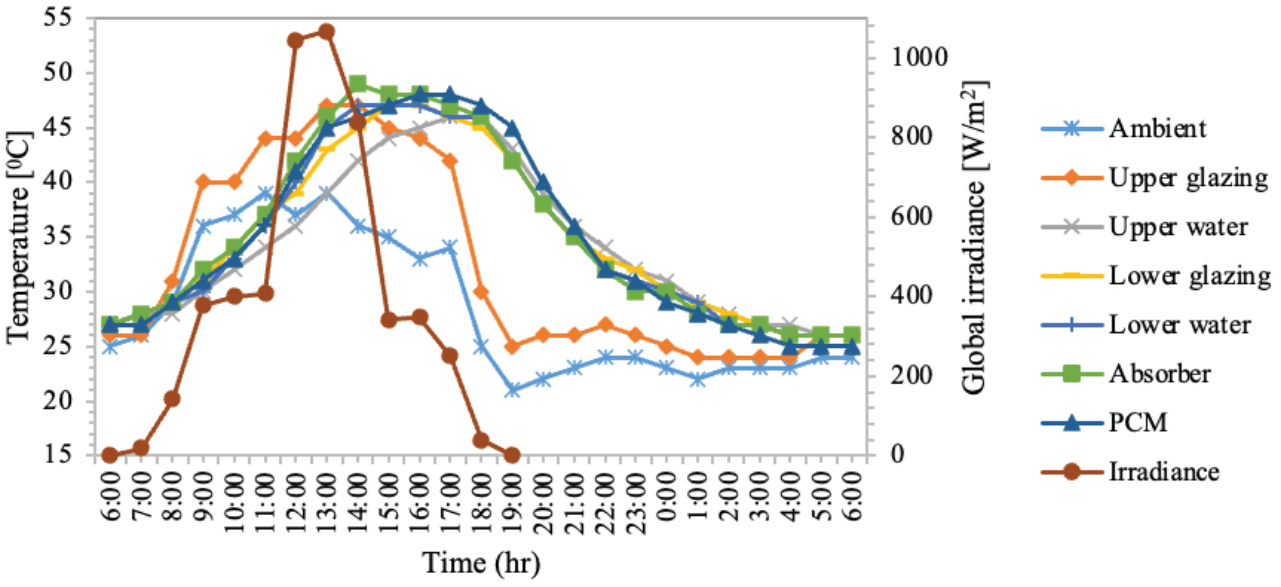

Figure 8. 24-hour temperature profiles of the still components with solar radiation on 3rd of March 2020.

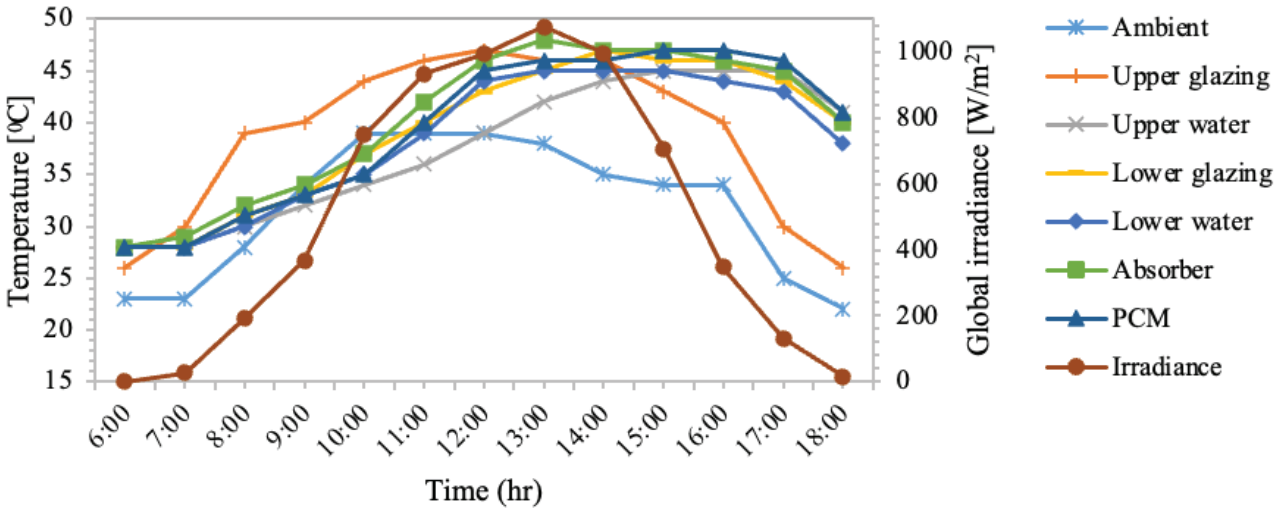

Figure 9. Temperature profiles of the still components with solar radiation on 13th March 2020.

in the ambient temperature with resultant improvement in temperature differentials in the system. Maximum solar radiation values of 1067 and 1077 W/m² were recorded at 13:00 hours on the 3rd and 13th of March, respectively. This month recorded higher values in solar radiation compared to February due to the reduction in ambient particulate matter and the improvement in atmospheric visibility and as such, the system recorded improved temperature values in March.

From Figure 8, The PCM attained a peak temperature of 48 °C and maintained dominance from 17:00 to 22:00 hours, thus serving as the energy source in the system during this period. The presence of the upper and lower condensing covers prevented the escape of long-wave radiation from the upper saline water (greenhouse effect). This development explains the relatively high-temperature values maintained by the upper saline water towards sunset, and the subsequent sustenance of the lower glazing's temperature, especially during the off-sunshine period.

Rainy Season Thermal Performance of the Still Components

The rainy season in Nigeria is characterized by cloudy and humid weather, fluctuating solar radiation, and increased levels of precipitation. The results obtained during this period are presented in Figures 10-13.

The thermal performance of the double-effect still during the rainy season is represented by Figures 10-13.

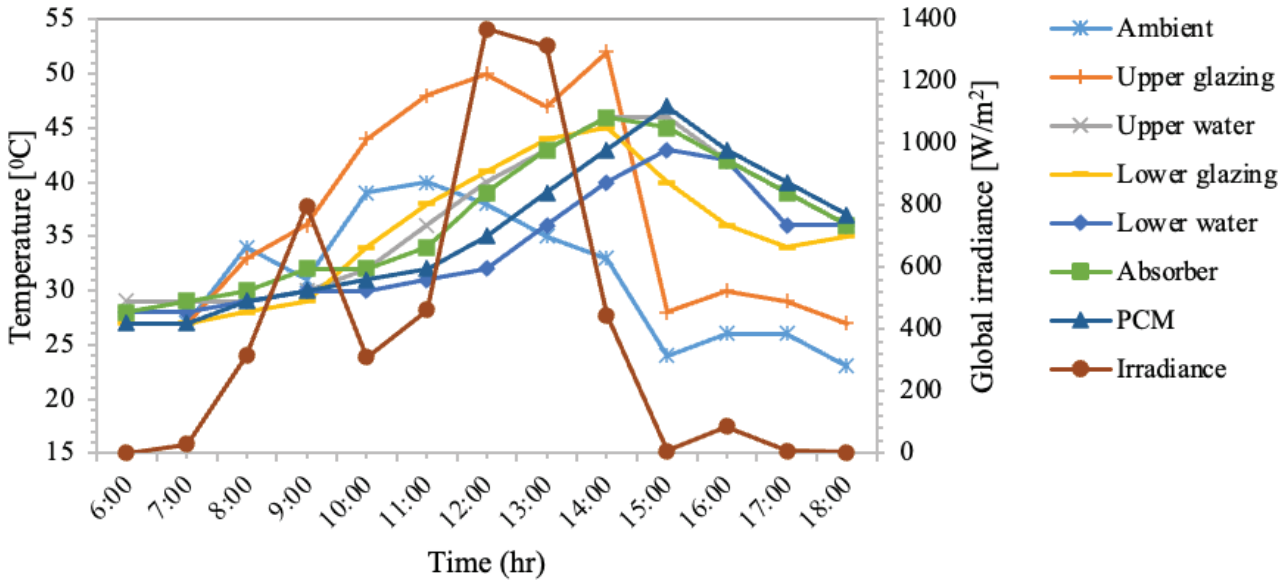

Figure 10. Temperature profiles of the still components with solar radiation on 10th April 2020.

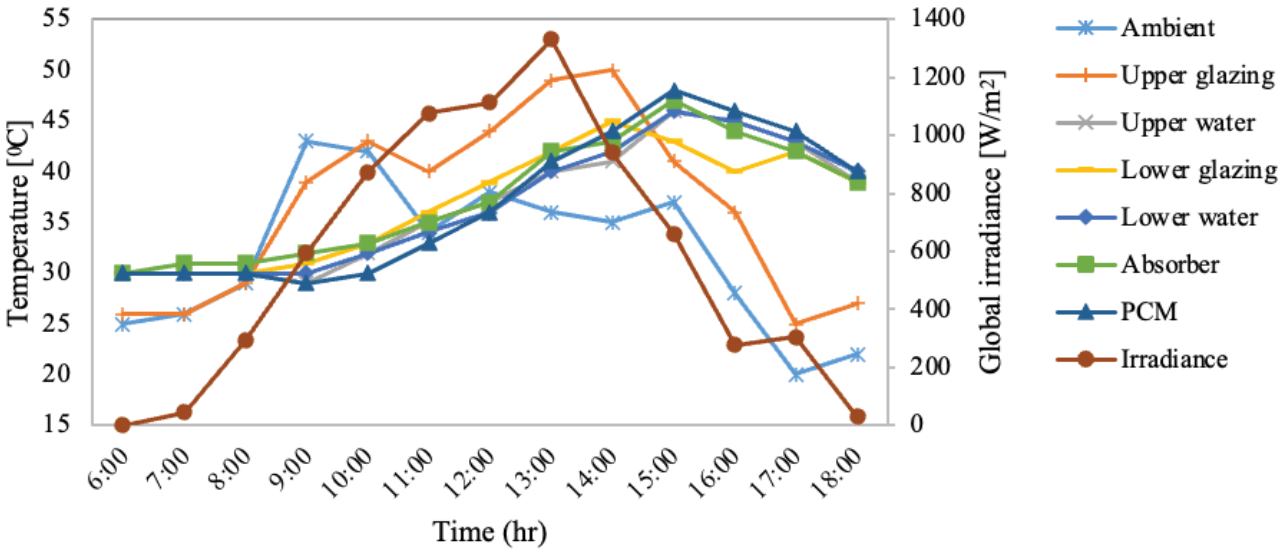

Figure 11. Temperature profiles of the still components with solar radiation on 6th May 2020.

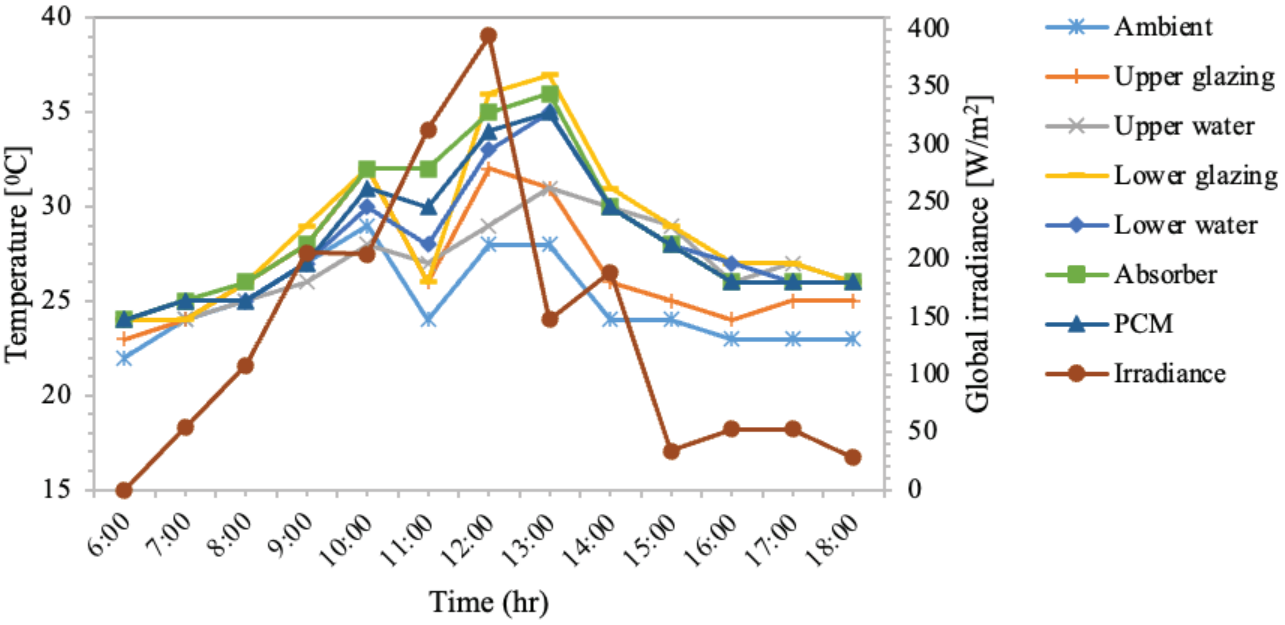

Figure 12. Temperature profiles of the still components with solar radiation on 7th July 2020.

These figures show the variation of the ambient and components' temperatures in response to the solar radiation intensity. From these figures, the degree of variation of solar radiation is associated with the yearly seasonal rainfall which spans from April to October. The temperatures of the still components varied similarly with the solar radiation and the ambient temperature. This shows the dependency of the temperature of the still components on the prevailing weather conditions.

Figures 10 and 11 represent the temperature profiles of the solar still components for April and May, respectively. From Figure 10, the dominance of the upper glazing's temperature spanned from 7:00 to 14:00 h with a peak solar radiation value of 1370 W/m^2. Similarly, from Figure 11, the upper glazing maintained a dominant temperature from 10:00 to 15:00 h with a maximum solar radiation value of 1332 W/m^2. The upper glazing is exposed to the ambient, and such responds faster to changes in ambient conditions. The system recorded maximum saline water temperatures of 47 and 46 °C in April and May, respectively. April and May mark the beginning of the rainy season in Nigeria. These months were mostly sunny with high solar radiation intensity and cloudy in the latter part of the day. This development impacted positively on the performance of

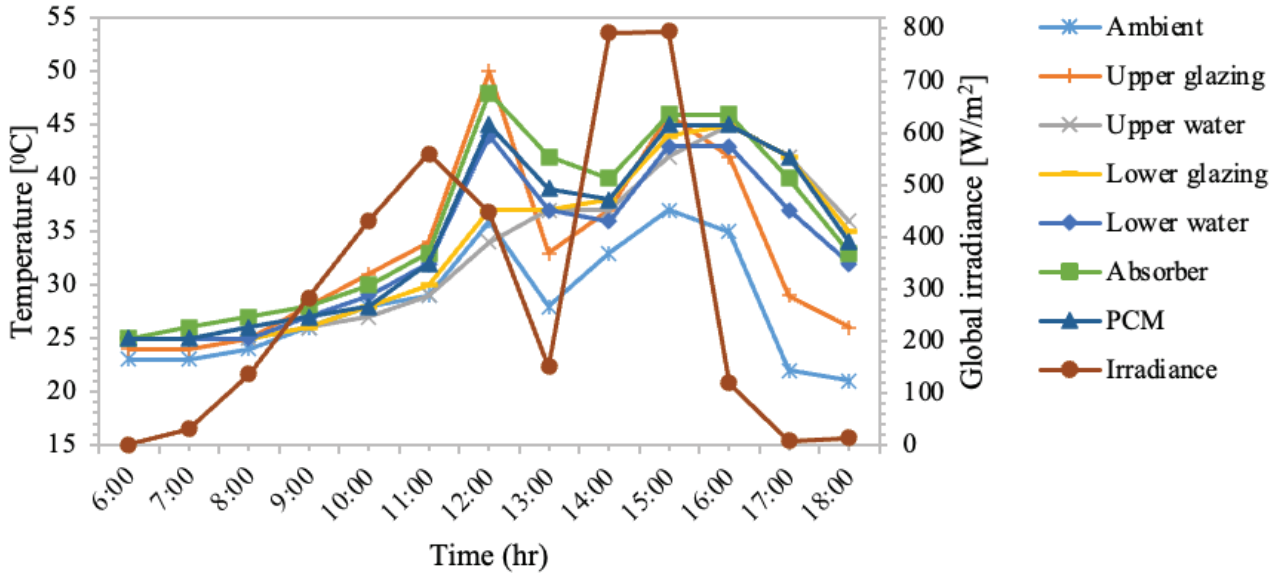

Figure 13. Temperature profiles of the still components with solar radiation on 10th October 2020.

the system with improved temperature differentials particularly, toward sunset.

Figures 12 and 13 represent the temperature profiles of the solar still components for July and October, respectively. From Figure 12, the solar still components recorded low temperatures with a maximum solar radiation value of 394 W/m². However, from Figure 13, the temperatures of the solar still components improved with a peak solar radiation value of 795.4 W/m². July and October were mostly cloudy and humid, thus recording low radiation values which hampered the performance of the system during this period. The system recorded maximum saline water temperatures of 35, and 44 °C in July and October, respectively. The cloudy/overcast weather experienced in July, particularly on the 7th day, prevented the system from gaining enough heat momentum, hence the low saline water temperatures recorded in this month.

Distillate Yield Distribution

Figures 14-16 show the twenty-four-hour distillate yield profiles of the upper and lower basins of the double-effect solar still in response to the variation of the solar radiation

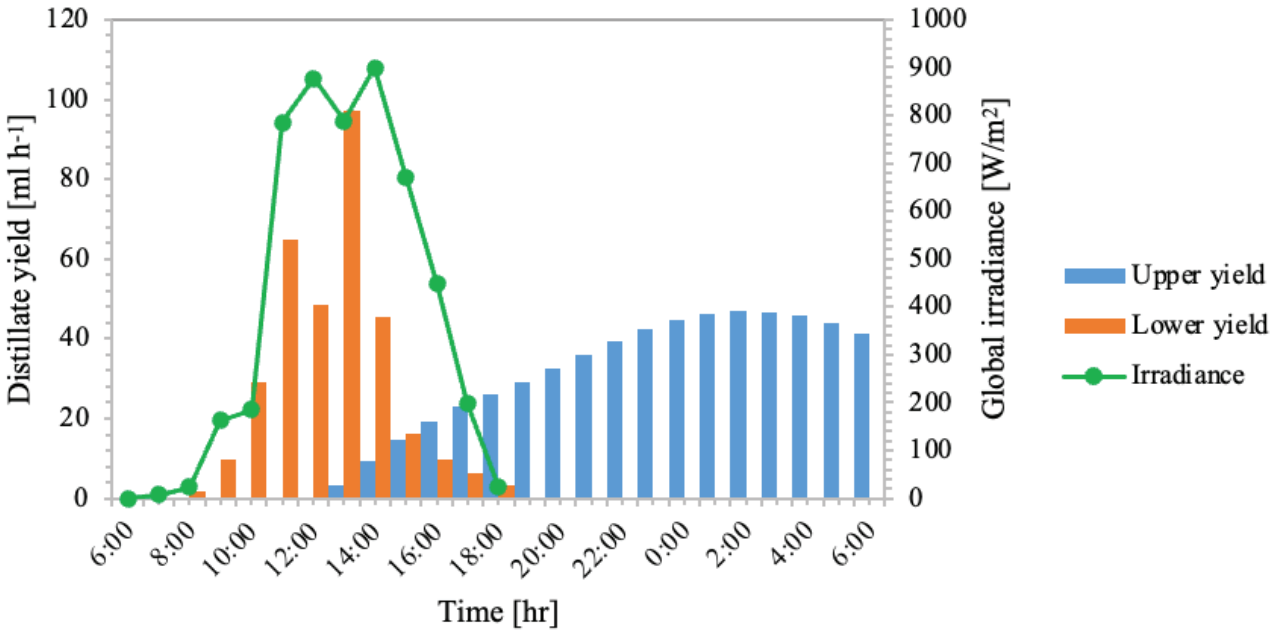

Figure 14. Twenty-four-hour distillate yield profile of the upper and lower basins on 10th February 2020.

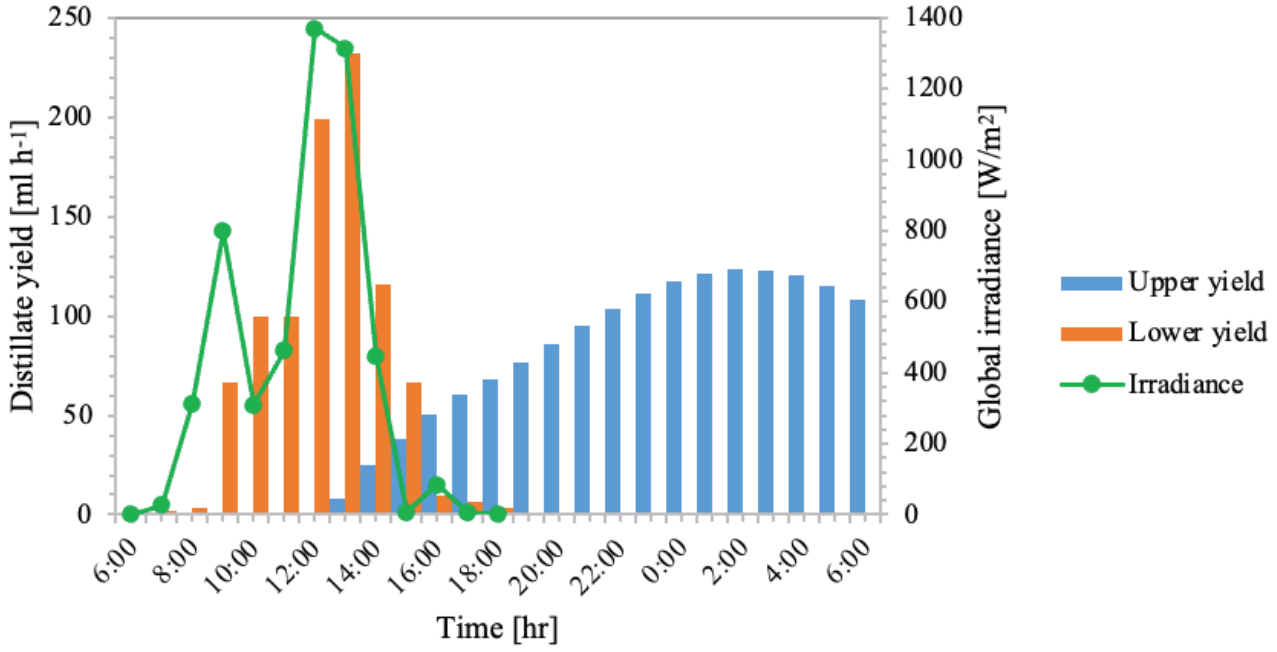

Figure 15. Twenty-four-hour distillate yield profile of the upper and lower basins on 4th May 2020

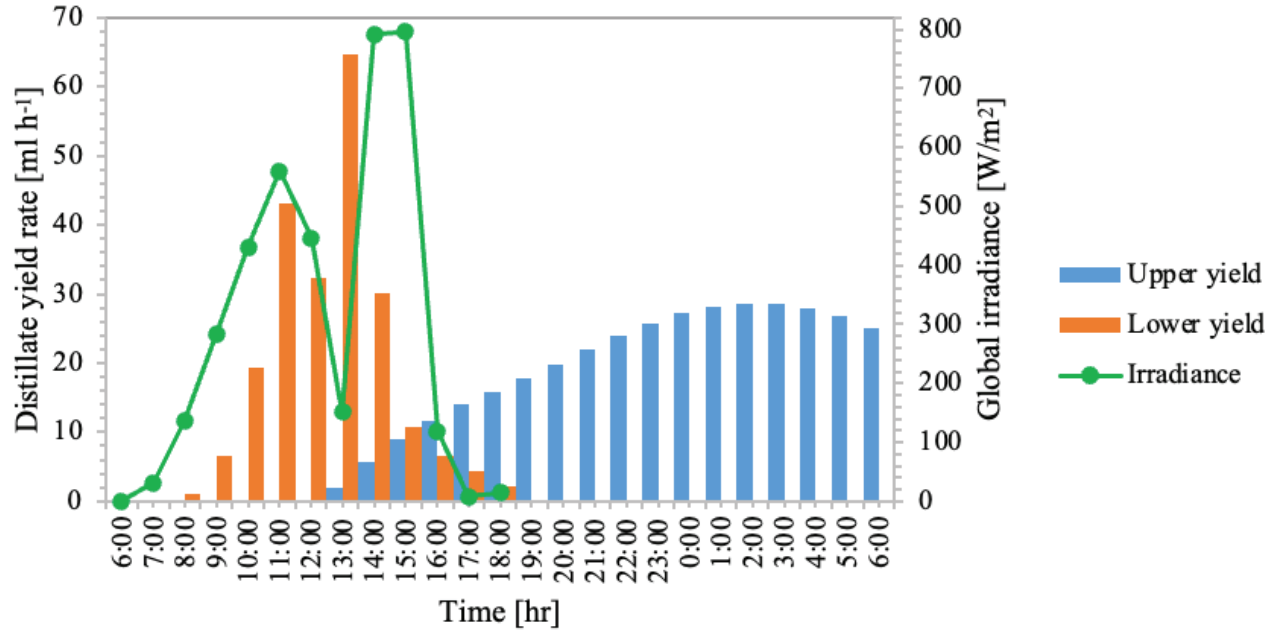

Figure 16. Twenty-four-hour distillate yield profile of the upper and lower basins on 8th October 2020.

during typical test days in February, May, and October, respectively.

From Figures 14-16, the lower basin commenced the production of freshwater ahead of the upper basin. This delay was due to the high-temperature values recorded by the upper glazing earlier in the day. The increase in solar radiation intensity increased the evaporation rate of the saline water, and consequently, increased the temperature of the humid air. The condensation of the humid air is initiated at the point where its dew point temperature is greater than the temperature of the glazing. Thus, the amount of condensed freshwater is a function of the temperature difference between the humid air and the glazing [26, 27]. This temperature difference was further improved with a decline in ambient temperature, particularly for the upper basin due to the exposure of its glazing. As such, the productivity

Table 5. Yield comparison of different double-effect solar still designs

S/No	Design	Yield (ml/m²)	Efficiency (%)	Reference
1	Inclined double basin still	2300	39.1	Pareshi et al. [29]
2	Double-basin single-slope still	2024	24.6	Modi et al. [30]
3	Double-basin hybrid still	840	11.7	Shukla and Modi [31]
4	Stepped upper basin with acrylic strips	2855	25.0	El-Sebaey et al. [32]
5	Integrated with paraffin wax PCM	2450	32.2	Present study

of the system extended beyond sunset. Though the PCM showed dominance in temperature during the nocturnal phase, the presence of the lower glazing overshadowed its performance. This was attributed to the heat retention ability of lower glazing which subsequently, retarded the condensation of humid air in the lower compartment.

The system recorded a maximum yield rate of 97 ml/h and a total daily yield of 920 ml on 10th February. The low yield can be attributed to the effect of the harmattan haze which limited visibility and radiation on the test day, thus the system didn't gain enough thermal energy for adequate distillate production. Similarly, working with single-effect stills, Ogunseye et al. [28] and Egarievwe et al. [20] achieved diurnal yield rates of 45 and 75 ml/h, respectively, during the harmattan period in Nigeria. The productivity of the system increased in May due to improved atmospheric visibility and recorded a maximum yield rate of 232.5 ml/h and a daily yield of 2,450 ml on the 4th day. However, the performance of the system declined in October due to the cloudy and humid weather that characterized the month. The system recorded a maximum yield rate of 64 ml/h and a daily yield of 580 ml on the 8th of October. A comparison of the maximum daily yields of selected works on double-effect solar still and the present study is shown in Table 5.

From Table 5, notwithstanding the effects of climatic conditions and design configurations, it is plausible to say that the present study competed favourably with reported works in the literature. The percentage contributions of the diurnal and nocturnal yields in February, April, May, and October are shown in Figure 17.

From Figure 17, the nocturnal distillation which occurs after sunset constituted a larger percentage of the daily freshwater yield. The system was able to produce more distillate during the off-sunshine period due to the improved temperature difference between the upper saline water and the upper condensing cover occasioned by the sharp decline in ambient temperature. For a twenty-four-hour cycle, the nocturnal yield contributed about 55% of the total distillate yield. Nocturnal distillation dominates the freshwater yield of deep basin stills due to the stored thermal energy in the saline water mass before sunset [33]. Moreover, the high glazing temperature recorded during the day hampered the diurnal productivity of the still. From the work of Hamdan et al. [34], nocturnal yield contributed more than 50% of the daily freshwater production. This result is in line with the percentage nocturnal yield reported in this study. Similarly, Edeoja et al. [35] recorded 43% of the total distillate yield as nocturnal production. However, low nocturnal contributions were reported by Karthikeyan et al. [36]

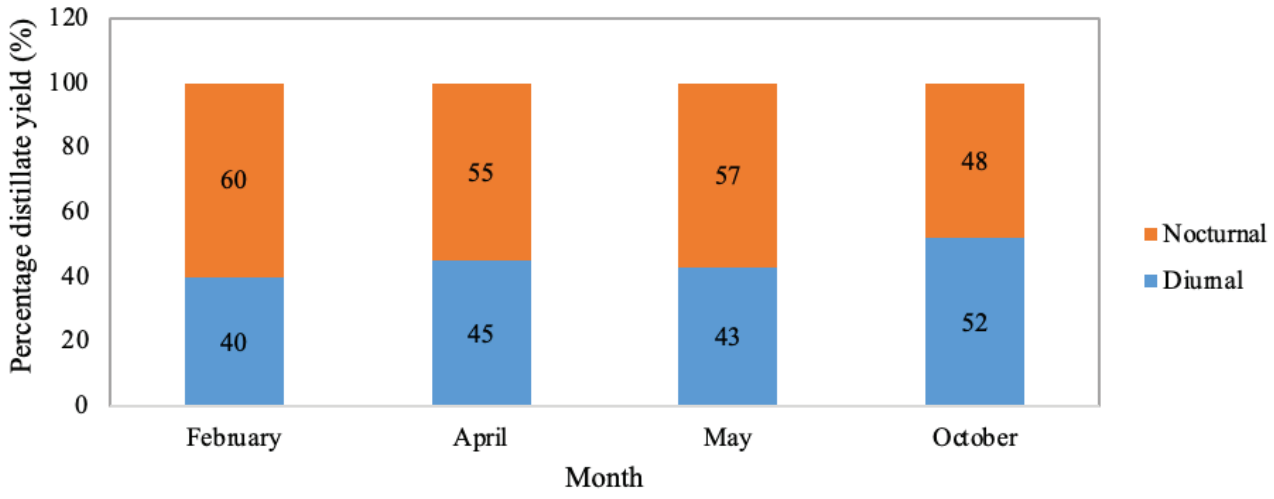

Figure 17. Diurnal vs Nocturnal percentage yields.

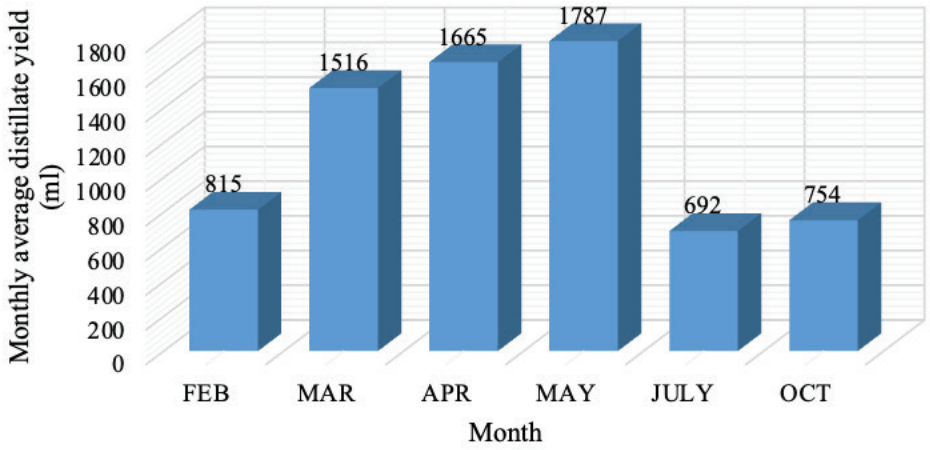

Figure 18. Monthly average distillate output.

and Agrawal and Rana [22]. This could be attributed to the prevailing ambient conditions. The average daily freshwater yields of the double-effect still for the months studied are presented in Figure 18.

From Figure 18, the months of February, July, and October had low average distillate yields despite the energy storage medium due to the poor weather conditions for these months. However, higher distillate volumes were obtained in March, April, and May primarily due to the high average solar radiation registered during these periods. Therefore, the intensity of solar radiation contributes greatly to the performance of solar stills.

Internal Heat Transfer Coefficients

Internal heat transfer involves the exchange of energy between the water interface and the inner surface of the glass cover. This energy exchange constitutes the convective, evaporative, and radiative heat transfers. The transfer coefficients were computed with Eqs. (A1), (A2), and (A3), respectively, and the results are presented in Figures19.

Figure 19 shows the variation of the convective, evaporative, and radiative heat transfer coefficients against the temperature difference between the saline water and the condensing surface. The evaporative heat transfer coefficient showed significant improvement with an increase in temperature difference. However, the convective and radiative heat transfer coefficients showed low values and less significance with an increase in temperature difference. Thus, the evaporative heat transfer mode constitutes the major energy transport from the saline water interface to the condensing cover.

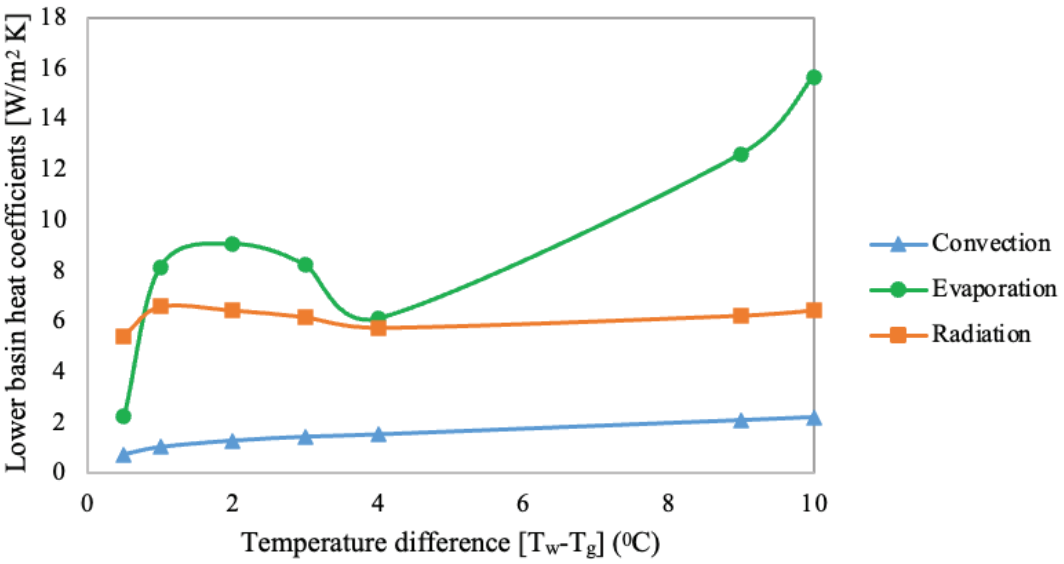

Figure 19. Heat transfer coefficients in the lower basin against temperature difference.

Table 6. Efficiencies of the double effect active solar still

S/No	Months	Daily irradiance (W/m²)	Daily yield (L)	Daily efficiency (%)
1	February	5009.2	0.920	12.43
2	March	5126.8	1.904	25.24
3	April	5023.4	2.300	31.35
4	May	5143.4	2.450	32.21
5	July	1713.3	0.367	14.46
6	October	4147.5	0.744	12.20

Efficiency

The efficiency of the system for representative days of the months considered was computed with the aid of Eq. (A8), and the values are presented in Table 6.

From Table 6, the efficiency of the double-effect still ranged from 12.20 to 32.21 % with an average value of 20 %. Similarly, Al-Karaghouli and Alnaser [6] recorded an efficiency range of 24.4 to 35.1 % with a double-effect still.

Economic Analysis

One of the criteria for determining the success of a project is its economic viability. Factors that affect the cost of solar-powered desalinated water include quality of feedstock, unit size, available solar radiation, final product quality, etc. The cost of the different components of the double-effect still is presented in Table 7.

The cost per litre of desalinated water (CLW) depends on the Annual Fixed Cost (AFC), Annual Maintenance Cost (AMC), Annual Salvage Value (ASV), and annual production capacity (Q) as defined by Eq. (7) [37, 22]:

Table 7. Fabrication fixed cost of the double-effect still

Material	Quantity	Cost ($)
Glass cover, 3.2 mm thickness	1.1m² (2 Nos)	20 (N8,200)
Galvanized steel sheet (2mm)	1.1m²	10 (4,100)
Wooden board	2.7m²	12 (N4,920)
Paint	1.5 litres	2 (N 820)
Base insulation (5 cm thick)	1.1 m²	3 (N1,230)
Supporting structure	1 unit	9 (N3,690)
Saline water Feedstock tank	35 litres	5 (N2,050)
Paraffin wax PCM	7kg	12 (N4,920)
Others	1 unit	10 (4,100)
Fabrication cost	1 unit	30 (N12,300)
Total Fixed Cost (TFC)	1 unit	113 (N46,330)

$$\mathrm{CLW} = \frac{\mathrm{AFC} + \mathrm{AMC} - \mathrm{ASV}}{Q} \tag{7}$$

The expression for the AFC is obtained from [22]:

$$\mathrm{AFC} = (\mathrm{CRF}) \times (\mathrm{TFC}) \tag{8}$$

where TFC is the Total Fixed Cost and CRF is the Capital Recovery Factor, and it is expressed as

$$\mathrm{CRF} = \frac{i(1+i)^n}{(1+i)^n - 1} \tag{9}$$

where i is the annual interest rate and n is the life cycle of the system.

From available literature [34, 38], the life span of a solar distillation unit is approximately 10 years. For the economic analysis of solar stills with a life cycle of 10 years, an annual interest rate of 3% is assumed [37]. The Annual Maintenance Cost (AMC) is assumed to be 30% of the Annual Fixed Cost (AFC) while the Annual Salvage Value (ASV) is expressed as [37]:

$$\mathrm{ASV} = \mathrm{SFF} \times \mathrm{SV} \tag{10}$$

where SV is the Salvage Value, and it accounts for about 20% of the Total Fixed Cost (TFC). SFF is the Sinking Fund Factor, and it is expressed as

$$\mathrm{SFF} = \frac{i}{(1+i)^n - 1} \tag{11}$$

The solar still performance during the rainy season is usually very poor due to the cloudy nature of the atmosphere and the low values of solar radiation reaching the earth. As such, it is plausible to assume 250 operating days per year [22]. Thus, with an average daily yield of 1.2 L/m², the annual production capacity (Q) is estimated as 300 L/m²/year. From Eqs. (8) – (11), the annual cost estimations of the double-effect still are evaluated, and the results are summarized in Table 8.

Table 8. Annual cost estimations of the double-effect still

S/No	Q (L/year)	CRF	AFC ($)	SV ($)	SFF	ASV($)	AMC ($)
1	300	0.1172	13.25	22.6	0.08723	1.9714	3.975

Substituting the values in Table 8 into Eq. (7), the cost of a litre of desalinated water (CLW) is estimated at $0.0508 per litre (20.83 N/L). For solar stills without graphene and precious metals, the cost per litre of fresh water (CLW) is within the range of 0.0061-0.277 $/L [39], which agrees with the freshwater cost of 0.0508 $/L reported in this study.

The Market Price (MP) of a litre of potable water in Nigeria is N150 ($0.366). Thus, the Annual Market Price (AMP) of purified water is expressed as

$$\mathrm{AMP} = \mathrm{Q} \times \mathrm{MP} \tag{12}$$

Thus, the Net Annual Earnings (NAE) is expressed as

$$\mathrm{NAE} = \mathrm{AMP} - \mathrm{AMC} \tag{13}$$

From Eq. (13), the Net Daily Earnings (NDE) is expressed as

$$\text{Net Daily Earnings (NDE)} = \frac{\text{Net Annual Earnings (NAE)}}{\text{Number of operating days}} \tag{14}$$

From Eq. (12), considering an annual production capacity (Q) of 300 L/year and a market price (MP) of $0.366 per litre, the annual market price (AMP) is estimated at $109.8. From Table 8, the annual maintenance cost (AMC) is $3.975, thus from Eq. (13), the net annual earnings (NAE) is estimated as $105.83. Substituting Eq. (13) into Eq. (14) and considering operating days of 250 per year, the net daily earnings (NDE) is estimated at $0.423.

The payback period (PP) shows the length of time required to recoup the initial cost expended on a project. It is also seen as the time required to reach the break-even point of investment. For solar still technology, the expression for the payback period (PP) in days is obtained from [22]:

$$\text{Payback Period (PP)} = \frac{\text{Total Fixed Cost (TFC)}}{\text{Net Daily Earnings (NDE)}} \tag{15}$$

From Table 7, the total fixed cost (TFC) is $113, while from Eq. (14), the net daily earnings (NDE) is $0.423. Thus, substituting these values into Eq. (15) gives the payback period for the double-effect solar still as 267 days.

The payback period of 267 days shows that the initial capital investment on the double-effect still can be recouped in less than a year. Comparing the market price of a litre of water (N150) in Nigeria to the cost of desalinated water (N20.83) plus an allowance for packaging cost shows that the system is economically viable and is suitable particularly, for low-income-earners.

The market for Solar-powered desalination is increasingly gaining relevance. This market is projected to evolve globally at a compound annual growth rate (CAGR) of 7.9% from 2019 to 2025 [40]. Considering the low yield of solar stills, the projected growth rate can be bettered through the design of efficient plants with large capacities. Hence, there is a need for a concerted effort in the production of freshwater at an affordable rate to meet the demands of the local populace.

CONCLUSION

An extended performance study of a double-effect active solar still with organic phase change material under the climatic conditions of Owerri has been undertaken. From this study, the following conclusions are drawn

- ✓ Results obtained showed that the temperature profiles of the still components mimicked that of the solar radiation with respective time lags.
- ✓ It was observed that the lower basin commenced the production of distillate ahead of the upper basin. This was due to the high temperature of the top glazing that impeded the performance of the upper basin earlier in the day. Thus, the lower basin had a better diurnal performance compared to the upper basin.
- ✓ The upper basin contributed a greater percentage of the nocturnal yield due to the exposure of the top condensing cover to the cooler ambient environment.
- ✓ The nocturnal yield constituted about 55% of the total freshwater yield. This was attributed to the improved temperature differentials in the upper compartment at night, and the sensible heat stored in the saline water mass before sunset.
- ✓ Amongst the months studied, the system recorded its best average performance in May and its least in July, and a maximum efficiency of 32.21%.
- ✓ The double-effect solar still studied, provides potable water in a decentralized manner with zero greenhouse gas emissions. For a life cycle of 10 years, the cost of freshwater production from the system is estimated at 0.0508 $/L with a payback period of 267 days. Thus, this system is an eco-friendly and cost-effective method of distilling fresh water from saline water.

APPENDIX

The convective, evaporative, and radiative heat transfer coefficients, respectively, from the water interface to the condensing surface are obtained from [37]:

$$h_c = 0.884\left[\left(T_w - T_g\right) + \frac{\left(P_w - P_g\right)\left(T_w + 273\right)}{268.9 \times 10^3 - P_w}\right]^{1/3} \tag{A1}$$

$$h_e = 16.276 \times 10^{-3} h_c \frac{P_w - P_g}{T_w - T_g} \tag{A2}$$

$$h_r = \varepsilon_e \sigma \left[\left(T_w + 273\right)^4 - \left(T_g + 273\right)^4\right]\left(T_w - T_g\right)^{-1} \tag{A3}$$

where, P_w and P_g are the vapour pressures at the water and condensing surface temperatures, respectively, and are expressed as:

$$P_{partial} = exp\left[25.317 - \frac{5144}{(T+273)}\right] \quad \text{(A4)}$$

The wind convective and radiative heat loss coefficients from the upper glazing to the ambient are obtained from [41]:

$$h_{w\,g2-a} = 2.8 + 3v \quad \text{(A5)}$$

$$h_{r\,g2-a} = \frac{\varepsilon_g \sigma (T_{g2} + T_s + 546)\left[(T_{g2}+273)^2 + (T_s+273)^2\right](T_{g2}-T_s)}{(T_{g2}-T_a)} \quad \text{(A6)}$$

where v is the prevailing wind velocity and T_s is the sky temperature, expressed in terms of the ambient temperature, T_a as [37]:

$$T_s = 0.052 \times T_a^{1.5} \quad \text{(A7)}$$

The relation for daily thermal efficiency of the system is obtained from [24]:

$$\eta_d = \frac{\dot{m}_d \times h_{fg}}{\sum I(t) \times 3600 \times A_{ab}} \quad \text{(A8)}$$

where $\dot{m}_d$ is the daily distillate yield of the system (Kg/day), T_{fg} is the latent heat of vaporization of water (J/kg), $\sum I(t)$ is the summation of the solar radiation per day (W/m^2.day) and A_{ab} is the absorber area (m^2).

NOMENCLATURE

A	Area (m^2)
h	Heat transfer coefficient (W/m^2.K)
h_{fg}	Latent heat of vaporization (J/kg)
H	Daily solar irradiation (J/m^2.day)
I(t)	Solar radiation intensity (W/m^2)
k	Thermal conductivity (W/m.K)
$\dot{m}_d$	Daily distillate yield (kg/day)
P	Vapor pressure (N/m^2)
Q	Energy (J/m^2.day), Annual production capacity (L/m^2.year)
T	Temperature (°C)
U	Internal uncertainty
X	Thickness (m)
v	Wind speed (m/s)
α	absorptivity
ε	Emittance
η_d	Daily efficiency (%)
τ	transmittance
σ	Stefan-Boltzmann constant (W/m^{2}K^4), Standard deviation

Subscripts

a	Ambient
ab	Absorber
c	Convection
e	Evaporation, effective
g	Glazing
r	Radiation
s	Sky
T	Tilted surface
w	Water, wind
1	Lower basin
2	Upper basin

Abbreviations

CSS	Conventional Solar Still
PCM	Phase Change Material
PP	Payback period
SSASS	Single Slope Active Solar Still

AUTHORSHIP CONTRIBUTIONS

Authors equally contributed to this work.

DATA AVAILABILITY STATEMENT

The authors confirm that the data that supports the findings of this study are available within the article. Raw data that support the finding of this study are available from the corresponding author, upon reasonable request.

CONFLICT OF INTEREST

The author declared no potential conflicts of interest with respect to the research, authorship, and/or publication of this article.

ETHICS

There are no ethical issues with the publication of this manuscript.

REFERENCES

[1] UNICEF. Nigerian children do not have enough water to meet their daily needs [Internet]. Available at: https://www.unicef.org/nigeria/press-releases/nearly-one-third-nigerian-children-do-not-have-enough-water-meet-their-daily-needs Last Accessed Date: 17.10.2021.

[2] Majcher K. How can desalination become cheaper? MIT Technology Review. 2014. Available at: https://www.google.com/amp/s/www.technologyreview.com/2014/12/03/170231/how-can-desalination-become-cheaper/amp/ Last Accessed Date: 16/10/2021.

[3] Kedar SA, Raj KA, Bewoor AK. Performance analysis of hybrid solar desalination system using ETC and CPC. SN Appl Sci 2019;1:965. [CrossRef]
[4] Mouhsin N, Bouzaid M, Taha-Janan M. Experimental analysis of an improved cascade solar desalination still with modified absorber plate. E3S Web of Conferences 2022;336:1-5. [CrossRef]
[5] Diabil HAN. Experimental study to enhance the productivity of single-slope single-basin solar still. Open Eng 2022;12:157-168. [CrossRef]
[6] Al-Karaghouli AA, Alnaser WE. Performances of single and double basin solar-stills. Appl Energy 2004;78:347-354. [CrossRef]
[7] Agboola OP, Atikol U, Assefi H. Feasibility assessment of basin solar stills. Int J Green Energy 2015;12:139-147. [CrossRef]
[8] Panchal HN. Enhancement of distillate output of double basin solar still with vacuum tubes. J King Saud Univ Eng Sci 2015;27:170-175. [CrossRef]
[9] El-Sebaey MS, Ellman A, Hegazy A, Panchal H. Experimental study and mathematical model development for the effect of water depth on water production of a modified basin solar still. Case Stud Therm Eng 2022;33:1-13. [CrossRef]
[10] Zurigat YH, Abu-Arabi MK. Modelling and performance analysis of a regenerative solar desalination unit. Applied Therm Eng 2004;24:1061-1072. [CrossRef]
[11] Madhlopa A, Johnstone C. Numerical study of a passive solar still with separate condenser. Renew Energy 2009;34:1668-1677. [CrossRef]
[12] Elsharif N, Mahkamov K. Multi-effect solar water still with evaporation pressure self-reduction capability. J Clean Energy Technol 2018;6:139-142. [CrossRef]
[13] Sonker VK, Chakraborty JP, Sarkar A, Singh RK. Solar distillation using three different phase change materials stored in a copper cylinder. Energy Rep 2019;5:1532-1542. [CrossRef]
[14] El-Sebaii AA, Al-Ghamdi AA, Al-Hazmi FS, Faidah AS. Thermal performance of a single basin solar still with PCM as a storage medium. Appl Energy 2009;86:1187-1195. [CrossRef]
[15] Kabeel AE, Abdelgaied M, Mahgoub M. The performance of a modified solar still using hot air injection and PCM. Desalination 2016;379:102-107. [CrossRef]
[16] Ramasamy S, Sivaraman B. Heat transfer enhancement of solar still using phase change materials (PCMs). Int J Eng AdvTechnol 2013;2:597-600.
[17] Safaei MR, Goshayeshi HR, Chaer I. Solar still efficiency enhancement by using graphene oxide/paraffin Nano-PCM. Energies 2019;12:1-13. [CrossRef]
[18] Sharshir SW, Peng G, Wu L, Essa FA, Kabeel AE, Yang N. The effect of flake graphite nanoparticles, phase change material, and film cooling on the solar still performance. Appl Energy 2017;191:358-366. [CrossRef]
[19] Boubekri M, Chaker A. Yield of an improved solar still: numerical approach. Energy Proced 2011;6:610-617. [CrossRef]
[20] Egarievwe SU, Animalu AOE, Okeke CE. Harmattan performance of a solar still in the guinea savannah. Renew Energ 1991;1:799-801. [CrossRef]
[21] Ogunseye OD, Oladepo KT. Performance analysis of a basin-type solar still during harmattan. Drinking Water Eng Sci 2022. [Preprint]. doi: 10.5194/dwes-2021-19, 2022. [CrossRef]
[22] Agrawal A, Rana RS. Theoretical and experimental performance evaluation of single-slope single-basin solar still with multiple V-shaped floating wicks. Heliyon 2019;5:1-38. [CrossRef]
[23] Khaparde SA, Bhuibhar AG, Pande PP. Design and performance of solar still. Int J Eng Sci Res Technol 2018;7:291-306.
[24] Prasad AR, Sathyamurthy R, Sudhakar M, Madhu B, Mageshbabu D, Manokar AM, et al. Effect of design parameters on fresh water produced from triangular basin and conventional basin solar still. Int J Photoenergy 2021;2021:6619138. [CrossRef]
[25] Gaur MK, Tiwari GN, Singh P, Kushwah A. Heat transfer analysis of hybrid active solar still with water flowing over glass cover. J Therm Eng 2021;7:1329-1343. [CrossRef]
[26] Nwosu EC, Nwaji GN, Ononogbo C, Ofong I, Nwadinobi PC, Ogueke NV, et al. Numerical and Experimental study of a single-slope double-effect solar still integrated with paraffin wax. Energy Nexus 2022;8:100155. [CrossRef]
[27] Bao N. The Mathematical Model of Basin-Type Solar Distillation Systems. London: Intechopen; 2019. [CrossRef]
[28] Ogunseye O, Omole-Adebomi A, Salami S. Performance analysis of a basin-type solar still during harmattan- raw data. Amsterdam: Mendeley Data, Elseiver; 2021. [CrossRef]
[29] Pareshi PR, Dhande KK, Bhagat G, Suvarnkar V, Javanjal V. Solar water distillation system by using inclined double basin. Int Res J Eng Technol 2019;6:1310-1313.
[30] Modi KV, Ankoliya DB, Shukla DL. An approach to optimization of double basin single slope solar still water depth for maximum distilled water output. J Renew Sustain Energy 2018;10:043708. [CrossRef]
[31] Shukla D, Modi K. Hybrid solar still as a co-generative system and desalination system - an experimental performance evaluation. Clean Eng Technol 2021;2:1-12. [CrossRef]
[32] El-Sebaey MS, Hegazy A, Ellman A, Ghonim T. Experimental and CFD study on single slope double basin solar still. Eng Res J 2021;44:21-32. [CrossRef]
[33] Onyegegbu SO. Nocturnal distillation in basin-type solar stills. Appl Energy 1986;24:29-42. [CrossRef]

[34] Hamdan MA, Al Momani AM, Ayadi O, Sakhrieh AH, Manzano-Agugliaro F. Enhancement of solar water desalination using copper and aluminum oxide nanoparticles. Water 2021;13:1914. [CrossRef]
[35] Edeoja AO, Ibrahim JS, Adaba S. Contribution of night time yield to the overall water production capacity of a simple basin solar still under Makurdi climate. Am J Eng Res 2013;2:32-43.
[36] Karthikeyan J, Selvaraj P, Nagaraj G. Day and night yield performance analysis of solar still for saline water using energetic materials with thermocol insulation. Mater Today Proc 2020;33:4848-4851. [CrossRef]
[37] Johnson A, Mu L, Park YH, Valles DJ, Wang H, Xu P, Kota K, Kuravi S. A thermal model for predicting the performance of a solar still with Fresnel lens. Water 2019;11:1-20. [CrossRef]
[38] Abdullah AS, Omara ZM, Alarjani A, Essa FA. Experimental investigation of a new design of drum solar still with reflectors under different conditions. Case Stud Therm Eng 2021;24:100850. [CrossRef]
[39] Fu H, Dai M, Song H, Hou X, Riaz F, Li S, et al. Updates on evaporation and condensation methods for the performance improvement of solar stills. Energies 2021;14:7050. [CrossRef]
[40] Saxena A, Cuce E, Kabeel AE, Abdelgaied M, Goel V. A thermodynamic review on solar stills. Sol Energy 2022;237:377-413. [CrossRef]
[41] Duffie JA, Beckman WA. Solar Engineering of Thermal Processes. 4th ed. New York: John Wiley & Sons Inc.; 2013. [CrossRef]